Communications in Nonlinear Science and Numerical Simulation 123 (2023) 107294

Contents lists available at ScienceDirect

Communications in Nonlinear Science and Numerical Simulation

journal homepage: www.elsevier.com/locate/cnsns

Research paper

Bifurcation analysis and complex phenomena in self-excited microcantilevers

Matilde Gelli [a], Joao Mouro [b,1,2], Paolo Paoletti [c], Bruno Tiribilli [b,1,2], Michele Basso [a,*]

[a] Department of Information Engineering, University of Florence, via di Santa Marta 3, Florence, 50139, Italy
[b] Institute for Complex Systems, National Research Council (ISC-CNR), via Madonna del Piano 10, Florence, 50019, Italy
[c] School of Engineering, University of Liverpool, Brownlow Hill, Liverpool, L69 3GH, United Kingdom

ARTICLE INFO

Article history:
Received 7 September 2022
Received in revised form 29 March 2023
Accepted 28 April 2023
Available online 5 May 2023

Keywords:
DDE-Biftool
Microcantilever
Bifurcations
Frequency jumps

ABSTRACT

Sensors based on self-excitation of microcantilevers have been proposed as effective devices for the measurement of rheological properties of the fluid where they are immersed. However, embedding microcantilevers in a feedback loop causes complex phenomena that need to be investigated. Specifically, a variable delay in the loop originates jumps in the oscillation frequency. In this paper, we study the nonlinear dynamics of a self-excited microcantilever oscillating in viscous fluids. Using DDE-Biftool, a Matlab package for numerical bifurcation analysis of DDEs, we investigate the bifurcations of periodic solutions in one and two parameters. The numerical results are compared with some experimental data of previous studies.

1. Introduction

Microcantilevers-based platforms have been recently proposed as convincing tools for mass sensing applications and detectors for the rheological properties of the environment in which they are immersed [1–7]. Due to their tiny dimension (of the order of some μm), they allow real time measurement for very small volumes of the surrounding fluid and with high sensitivity. In particular, concentration of molecules of interest, as well as changes in the viscosity of the fluid, can be detected by measuring shifts in the resonance frequency of the oscillating cantilever [4–7]. In order to detect these shifts, one may use two different strategies: open loop or closed loop circuits. In an open loop circuit the cantilever is excited by using an external excitation. However, there are some drawbacks associated to this strategy such as the frequency scan required to determine the peak shift which results in a hard task due to the presence of spurious peaks when operating in viscous fluids. In order to overcome these difficulties, feedback strategies have been suggested, [8]. In this case, the cantilever is embedded in a feedback loop and it is self-excited by using a feedback signal which is proportional to the displacement (or velocity) of the cantilever itself [3,8]. Even if feedback strategies show some advantages, such as higher signal to noise ratio, compared to the open loop counterpart, on the other hand they cause some undesired behaviors due to the nonlinear nature of such kind of circuits. For instance, some authors implemented feedback strategies using a

* Corresponding author.
E-mail address: michele.basso@unifi.it (M. Basso).

[1] This research was partially funded by the European Union's Horizon 2020 research and innovation programme under the Marie Skłodowska-Curie grant agreement No 842147.

[2] JM and BT wish to acknowledge the support of the European Union to the MARS project (No 842147) funded by the European Union's Horizon 2020 research and innovation programme.

https://doi.org/10.1016/j.cnsns.2023.107294

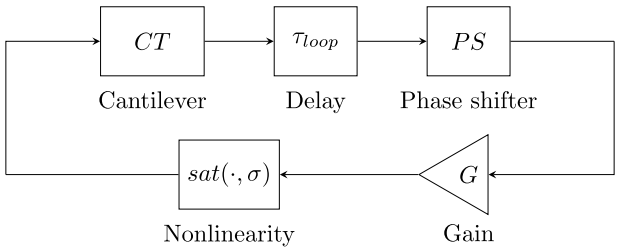

Fig. 1. Block diagram of the analyzed self-excited microcantilever system.

variable phase shifter [3–6,9], and they observed jumps in the frequency and amplitude of the oscillations as the phase was changed. These jumps are affected by the viscosity of the fluid [5]. In [6] the presence of a hysteresis region, related to the delay introduced in the system by the phase shifter, and whose width depends on the viscosity of the fluid, was verified.

These jumps have been studied using different strategies such as Harmonic Balance, Nyquist theorem [3], perturbation analytical techniques [4] or solving delayed differential equations [6], but some questions remain to be answered.

In this work, we try to explain such complex phenomena in terms of behavior of nonlinear dynamical systems and bifurcation theory. Indeed, frequency jumps can be explained by the occurrence of local bifurcations (sub-critical or catastrophic) which drive the cantilever to abruptly change amplitude and frequency of the current oscillation. In order to fully characterize bifurcations and complex behavior of the system, we use the Matlab package DDE-Biftool, a set of routines that can perform continuation of delayed differential equations [10–13].

Therefore, the paper is organized as follows: in Section 2 we provide a brief description of the physical system and introduce a suitable simplified mathematical model. This latter was a necessary step in order to generalize the problem and study the response of the system independently of the application. In Section 3 we explain how DDE-Biftool was set and works and in Section 4 we explain the types of bifurcations for a generic system. Section 5 bounds the bifurcations with the jumps and hysteresis region and in Section 6 we compare the theoretical results with some experimental data to prove the correctness of this study. A brief summary is given is Section 7.

2. System description and mathematical model

The system consists of a cantilever oscillating in a viscous fluid due to the effect of a feedback loop directly driven by the deflection signal. Amplitude and frequency of the oscillation generally depend both on microcantilever characteristics and fluid properties but can also be adjusted by the feedback electronics through a saturation circuit, a gain and a phase shifter which can be employed to optimize the operating conditions. The block diagram of the system is reported in Fig. 1.

The block τ_{loop} represents a general intrinsic delay in the loop which encloses all sources, for example, due to electronic components and the time needed to the acoustic wave to propagate from the piezo actuator to the beam.

The dynamics of this system can be described as the following forced damped harmonic oscillator

$$m\ddot{x}(t) + c\dot{x}(t) + kx(t) = -sat(Gx_{PS}(t - \tau_{loop}), \sigma) \tag{1}$$

where x is the deflection of the cantilever, m and c are the mass and damping coefficients respectively, while k is the spring constant. The right hand side of (1) is the force acting on the cantilever, where x_{PS} is the deflection signal after being fed to the phase shifter PS, $G > 0$ is the amplification gain of the feedback and $sat(\cdot, \sigma)$ represents the saturation function with σ being the saturation level. The minus sign before the saturation function means that a negative feedback is taken into account.

The system PS provides a tunable shift in the phase of the input signal without altering its amplitude and it can be easily implemented as the following first order all pass filter

$$x_{PS}(t) + \gamma\dot{x}_{PS}(t) = x(t) - \gamma\dot{x}(t) \tag{2}$$

where $x(t)$ and $x_{PS}(t)$ are the input and output signals, respectively, and the parameter γ is the filter time constant. By sweeping up and down γ, a shift in the phase of the signal is induced, see [3,6] for more details. For the sake of simplicity, we assume here that PS acts as an equivalent additional variable delay τ_{PS}, such that

$$x_{PS}(t - \tau_{loop}) \approx x(t - \tau_{loop} - \tau_{PS}) = x(t - \tau) \tag{3}$$

where $\tau = \tau_{loop} + \tau_{PS}$ is the total variable delay. Therefore, the dynamics (1) can be rewritten in a simplified form as

$$m\ddot{x}(t) + c\dot{x}(t) + kx(t) = -sat(Gx(t - \tau), \sigma) \tag{4}$$

Such a system can be frequently found in the literature [3–6,9,14], even though sometimes the saturation function may be replaced by the cubic nonlinearity [9,14], but the resulting system is equivalent, and it is always shown how it exhibits a particular behavior: when the delay τ is varied across a critical value, the beam oscillations abruptly change both in terms of frequency and amplitude. In particular, the system shows two branches of periodic solutions at different frequency, such that the cantilever can oscillate along one of them and then jumps to the other depending on τ [6]. Furthermore, experiments prove that these jumps in the response of the beam can be related to the rheological properties of the fluid in which the cantilever is immersed. Specifically, a variation in the viscosity of the medium leads to a shift of the critical values of the delay [5]. Although a deeper understanding of such behavior could be useful for the realization of rheometry and mass sensors, so far no study has analyzed the reason underneath the behavior described above. Therefore, in this paper a tool capable of performing bifurcation analysis of delayed differential equations (DDE-Biftool) was exploited to fill this knowledge gap. In fact, DDE-Biftool provides algorithms to make numerical bifurcation analysis of both steady state and periodic solutions (either stable and unstable solutions) of DDEs [10–13]. Concerning the periodic orbits, the tool is capable of: (i) compute the Floquet multipliers which give a measurement of the local stability of the periodic solution [15,16]; (ii) provide continuation of some type of bifurcations in two parameters such as fold and torus bifurcations.

Since the system described by Eq. (4) finds many applications in the literature, it is better to normalize it so that the governing equation applies to the whole range of applications. In addition, rewriting the equations in their dimensionless form is particularly useful in DDE-Biftool for two main reasons: (i) it allows a simpler definition of derivatives since a smaller number of parameters are present in the model, and (ii) the problem is better conditioned from a numerical point of view. In order to do this, let us define the new time variable $\bar{t} = \omega_n t$, where $\omega_n = \sqrt{k/m}$ is the natural frequency of the cantilever. Thus, Eq. (4) can be rewritten as

$$\ddot{x} + \frac{\dot{x}}{Q} + x = -\frac{1}{k} sat(Gx(\bar{t} - \bar{\tau})) \tag{5}$$

where $Q = \sqrt{mk}/c$ is the quality factor.

Further simplifications are needed to define and analyze the system using DDE-Biftool. In fact, DDE-Biftool requires the nonlinear functions to be smooth in order to evaluate the derivatives. Therefore, the saturation function $sat(\cdot, \sigma)$ has been approximated by the hyperbolic tangent as

$$sat(Gx(\bar{t} - \bar{\tau}), \sigma) \approx \sigma \cdot \tanh\left(\frac{G}{\sigma} x(\bar{t} - \bar{\tau})\right) \tag{6}$$

Then, substituting Eq. (6) in Eq. (5) yields

$$\ddot{x} + \frac{\dot{x}}{Q} + x = -\frac{\sigma}{k} \tanh\left(\frac{G}{\sigma} x(\bar{t} - \bar{\tau})\right) \tag{7}$$

which is in a form[3] suitable for implementation within DDE-Biftool.

Notice that the proposed model does not include possible geometric nonlinearities (such as the cubic Duffing term in the spring constant) sometimes considered in the mathematical formulation [17,18]. In fact, we are interested in studying the dynamics of the cantilever in viscous fluids, but in such kind of environment the cantilever deflections are small and they do not trigger those nonlinear behaviors. In addition, the oscillation amplitudes are restrained further by the presence of the saturation circuit, such that the hyperbolic tangent and the delay are considered sufficient for capturing the principle cantilever dynamics in this context.

3. Method

Without loss of generality, in the following we will analyze the system dynamics for a rectangular silicon tipless cantilever, the same utilized in [6]. The cantilever has density $\rho = 2.33 \times 10^3$ kg/m^3, length 160 μm, thickness 2.5 μm and width 33 μm. Just Q, G and $\bar{\tau}$ are defined as bifurcation parameters, while k and σ are kept fixed for the whole process. In fact, k depends just on the dimension of the cantilever and its material but not on the environment, instead the saturation level σ influences only the amplitude of the oscillations and it has to be carefully chosen to prevent the growth to be excessively large. It is worth noting that letting Q variable means that the viscosity of the fluid, as well as the additional masses on the probe, is allowed to change, making the environment dynamical. Table 1 reports the parameter values used to set up DDE-Biftool. We determined the value of parameter k experimentally by estimating first the mass of the cantilever (from the knowledge of its dimension and material) and then the natural frequency in air which, for this specific type, is found to be around 139.4 kHz.

As long as the gain G is small, the delayed differential equation defined by (7) has a locally stable equilibrium point in $(x, \dot{x}) = (0, 0)$. As G increases the above equilibrium undergoes an infinite number of Hopf bifurcations at $G = G_i$, $i \in N$,

[3] Eq. (7) could have been simplified further by introducing a normalization on the cantilever displacement as well, such as scaling the variable x with the cantilever length L itself [7,17], but this choice would not affect the number of bifurcation parameters

Table 1
Values of the parameters used in DDE-Biftool.

Parameter	Values	Units
k	0.0236	$\mu g/\mu s^2$
σ	0.1	$\mu g\ nm/\mu s^2$
$\hat{G}$	1	$\mu g/\mu s^2$
$\overline{\tau}$	3.8÷6.8	a.u.
Q	4.2÷28	a.u.

each giving birth to periodic solutions (limit cycles) with initial frequency ω_i. It is known [19] that all the pairs (G_i, ω_i) can be computed as the real and positive solutions (sorted in ascending order of G) of the complex characteristic equation

$$-\frac{k}{G} = \frac{e^{-j\omega\overline{\tau}}}{1-\omega^2+j\omega/Q}. \tag{8}$$

Typically, only the first two Hopf points are physically relevant as they are related to the periodic solutions seen experimentally. After having detected these points, the corresponding branches of limit cycles can be numerically continued as a function of G (see, e.g. [20]) until a sufficiently high value $\hat{G}$ is reached (see Table 1) to ensure the existence of the oscillations for every value of $\overline{\tau} > 0$ (a variation in the delay shifts the position of the Hopf points, therefore the oscillations would vanish if G is not large enough). Then, a second continuation is started for both limit cycles with respect to the delay $\overline{\tau}$ in order to analyze how the delay causes the jumps from one branch of periodic solutions to the other. The Matlab code for reproducing the results reported in the next sections is available on GitHub [21].

4. Bifurcation analysis varying the delay

In this section the two branches of periodic solutions, born from the first two Hopf points, are studied. For each of the branches we look for the bifurcations as the delay $\overline{\tau}$ is changed, and we will show how these may change for different values of the quality factor parameter Q. Therefore, let us fix Q at first, i.e. we set the environmental conditions a priori, and consider $\overline{\tau}$ as in Table 1.

4.1. Low frequency branch

The low frequency branch is the one that originates from the first Hopf point once the parameters σ, Q, k and G have been fixed. Fig. 2 shows the bifurcation diagrams for different values of Q (selected in the interval of interest for a wide range of fluids). On the x-axis there is the bifurcation parameter $\overline{\tau}$, while on the y-axis the amplitude defined as the maximum magnitude of the vector $(x, \dot{x})$ in the phase plane. This choice on the amplitude allows a more compact and cleaner representation of branches. In fact, all the solutions with symmetry properties on the phase plane and equal stability can be described by the same branch. A different color indicates a change in the number of unstable multipliers, which is indicated in the figure legend. Therefore, just the blue lines are stable, whereas the markers connecting profiles with different colors represent the bifurcation points. As one can notice, in each diagram there are many bifurcation points, but explicit labels have been given only to those relevant for the analysis presented in this paper. The others have been discarded since they involve unstable branches that cannot be neither seen experimentally nor simulated.

Starting from Fig. 2a, we see that the branch is initially stable and it remains stable until $\overline{\tau}$ =PF1, where a first bifurcation is found when one multiplier crosses the unit circle through +1. From the phase plane trajectories reported in Fig. 3 it is clear that a pitchfork bifurcation occurs, such that the stable symmetric limit cycle in Fig. 3(a) (solid line) becomes unstable in Fig. 3(b) (dashed line) and two asymmetric stable limit cycles originate from it (solid lines). In the bifurcation diagram of Fig. 2a the two branches related to the asymmetric limit cycles originating at PF1 overlap since the amplitude is exactly the same. These branches remain stable between PF1 and the fold bifurcation point F2, where the asymmetric limit cycles vanish due to the collision with the unstable branches originating from another pitchfork bifurcation at PF2.

Considering $Q = 11.5$ (see Fig. 2b) we notice that the pitchfork points PF1 and PF2 change from supercritical to subcritical and a new fold point F1 appears. In this case the stable branches are no longer connected in PF1 which means that slowly varying the delay around the PF1 bifurcation point triggers a transient that might lead towards a different attractor. The diagram does not change considerably if we keep on decreasing Q except for the fact that the two pitchfork points PF1 and PF2 get closer, leading to a reduction of the unstable region (Fig. 2c), until they hit around $Q = 6.8$. After the collision, the upper bifurcating branch detaches from the lower one, and an isolated closed structure is created, see Fig. 2d. We also notice that for small values of Q another fold point F3 appears (Figs. 2c-2f). If Q is swept down further, the lower frequency branch of Fig. 2d keeps its shape with F3 slightly shifting on the right, while for the closed structure F1 and F2 move closer (Fig. 2e) and finally disappears when $Q < 4.65$, due to the collision between the two fold points (Fig. 2f). Thus, when Q is sufficiently small, just one low frequency branch exists which loses its stability due to the fold bifurcation in F3 as the delay $\overline{\tau}$ is increased.

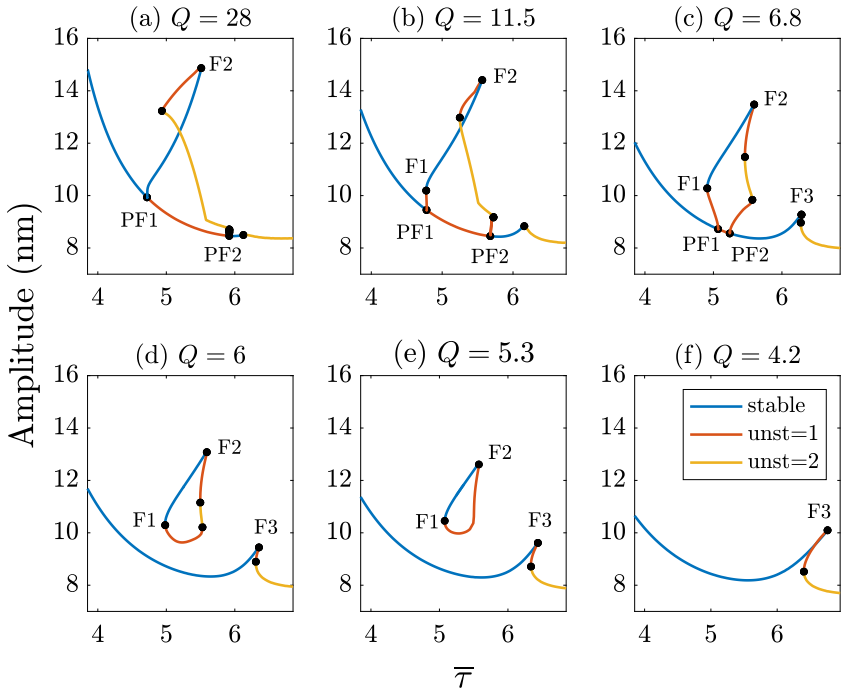

Fig. 2. Sequence of bifurcation diagrams for different values of the quality factor Q. Periodic solutions with opposite stability and number of unstable multipliers have been colored differently (just the blue lines are stable). The black dots represent bifurcation points and among them just the ones involving stable branches have been named.

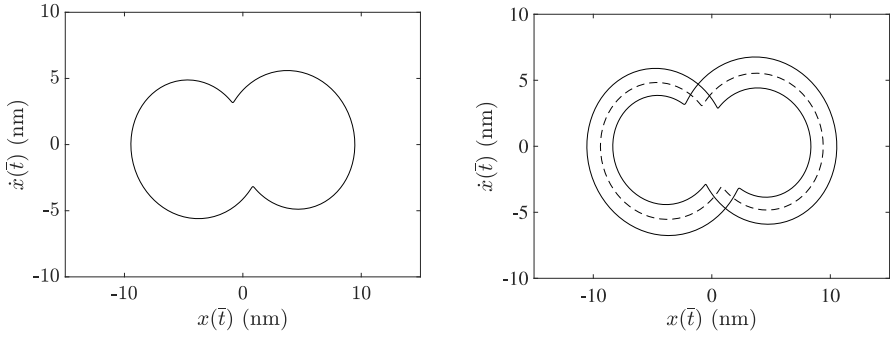

Fig. 3. Phase plane before (a) and after (b) the bifurcation point PF1. By convention, stable solutions are drawn with continuous lines and those unstable with dashed lines. After the bifurcation in PF1, two new stable asymmetric branches arise, while the previous stable solution becomes unstable.

In short, for the low frequency branch three scenarios are possible, according to the value of Q:

1. Existence of two pitchfork bifurcations connected via an auxiliary branch of asymmetric limit cycles ($Q > 6.8$);
2. The low frequency branch is split in two distinct parts ($4.65 \leq Q \leq 6.8$) with both of them presenting a stable region;
3. Just one low frequency branch exists ($Q < 4.65$).

4.2. High frequency branch

We now focus on the high frequency branch, i.e. the one originating from the second Hopf point. Unlike the low frequency branch, lowering Q does not cause a significant variation in the bifurcation diagram. In fact, one can verify that this branch always arises unstable and as the delay $\overline{\tau}$ is increased it switches to stability due to a secondary Hopf bifurcation, regardless of the parameter Q.

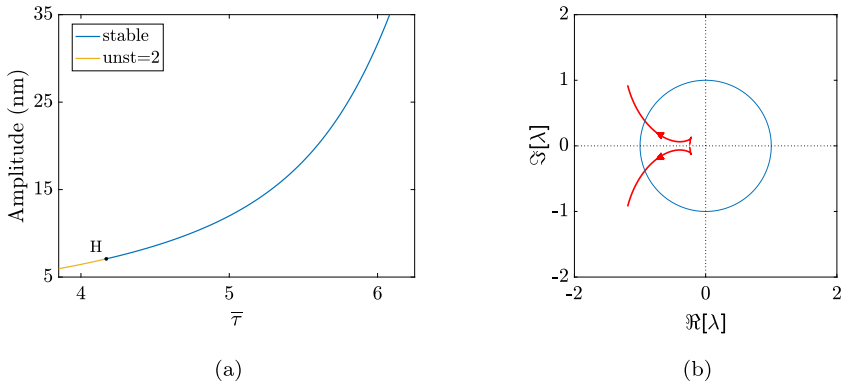

Fig. 4. In 4(a) the bifurcation diagram for the high frequency branch for any Q, while 4(b) represents how the Floquet multipliers λ_i move on the complex plane as $\overline{\tau}$ is varied. When the delay reaches the bifurcation point H, two multipliers become unstable by crossing the unit circle as shown in 4(b). Since the crossing happens far from the real axis, a secondary Hopf bifurcation occurs in H.

Table 2
High frequency branch: bifurcation point H as a function of Q.

Q	$\overline{\tau}$
28	4.186
22.41	4.171
11.53	4.172
6.58	4.179
5.5	4.19

A typical bifurcation diagram for this branch is plotted in Fig. 4(a).

As before, just the blue lines represent stable periodic solutions while the markers the bifurcation points. In this case, there is only one marker and since the periodic solution has two multipliers crossing the unit circle, (unst is equal 2 and those multipliers are shown in Fig. 4(b)), we can establish that in H a secondary Hopf bifurcation occurs. Furthermore, from the simulations we can prove that no other stable solutions are locally present. As a consequence, the bifurcation has to be subcritical.

For the high frequency branch changing Q simply implies a small shift in the occurrence of the bifurcation point H, but the bifurcation diagram is equivalent to the one of Fig. 4(a). For this reason we prefer to display in Table 2 directly the occurrences of point H for some values of Q.

5. Detection of jumps and the hysteresis region

Experiments show that in specific operating conditions the cantilever suddenly changes amplitude and frequency of the oscillations as the delay $\overline{\tau}$ is varied around some specific critical values [3,5]. Now, exploiting the results given in Section 4, we are able to explain this kind of complex phenomenon as a consequence of the bifurcation configuration of the system. In order to do this, we are considering two main cases according to the quality factor Q, i.e. $Q > 6.8$ and $Q \leq 6.8$, since different bifurcations are involved below and above that threshold.

5.1. Case Q above threshold

The high frequency branch only exhibits a secondary Hopf bifurcation for the explored range of $\overline{\tau}$ and Q, while the low frequency branch undergoes two pitchfork bifurcations which can be either supercritical and sub-critical. However, the following discussion only concerns the situation with sub-critical ones since it is the dominant type when $Q > 6.8$. In Figs. 5(a) and 5(b) bifurcation diagrams are reported for the amplitude and the (normalized) frequency $\overline{f}$, respectively.

Assume the cantilever is oscillating at a specific amplitude and frequency along the low frequency branch and the delay $\overline{\tau}$ is increased. Then, the solution follows the path as indicated by the black arrows in Fig. 5: it stays on the low frequency branch (LF branch) until it reaches point PF1 where a pitchfork bifurcation occurs. After this point the solution remains on the LF branch (the one bifurcating from PF1) until the branch vanishes due to the fold bifurcation in F2. When $\overline{\tau}$ is further increased, a transient force the solution to jump on the high frequency branch (HF branch) which is stable.

Once the solution is on the HF branch and the delay $\overline{\tau}$ is decreased the orbit evolves according to the red arrows until it experiences a jump from the HF branch to the LF branch as indicated by the red dashed line in point H where the secondary sub-critical Hopf bifurcation occurs. The red and black dashed arrows also delineate a hysteresis region which will be discussed in the following Section 6.

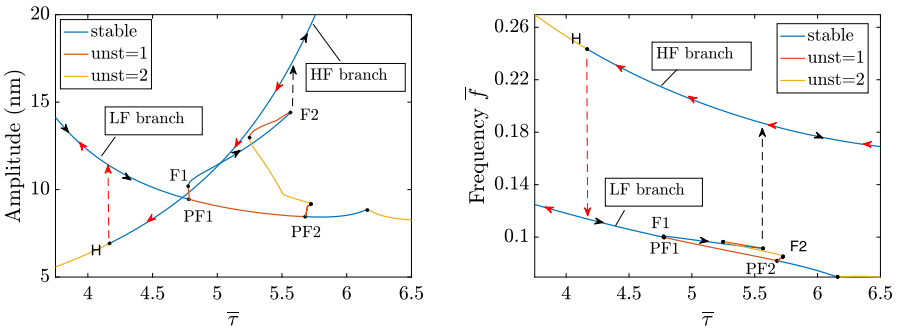

Fig. 5. Bifurcation diagrams in terms of amplitude (a) and normalized frequency $\overline{f}$ (b) when $Q > 6.8$. The black and red arrows indicate the evolution of the periodic solution as $\overline{\tau}$ is swept up and down, respectively. The labels "LF branch" and "HF branch" stand for low and high frequency branches.

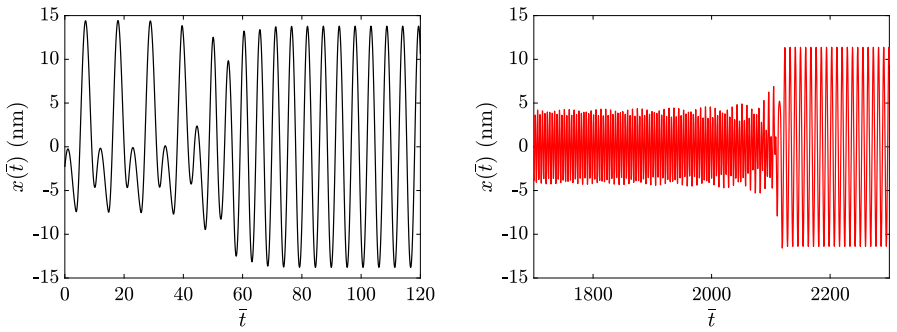

Fig. 6. Changes in the deflection of the cantilever $x(\overline{t})$ at the bifurcation points F2 and H, i.e. when the jumps from low to high and from high to low frequencies are triggered, respectively.

For the sake of clarity, we show in Fig. 6 the transient behaviors (in the normalized time domain) exhibited by the cantilever when the two jumps occur. In Fig. 6(a) we can see that the cantilever is initially oscillating following one of the two asymmetric periodic solutions at low frequency, but then it deviates quickly onto the new (symmetric) stable attractor at high frequency after the jump in F2. Fig. 6(b) displays instead how the HF branch becomes an unstable quasi-periodic solution after point H. In fact, we can distinguish the presence of a second frequency in the transient before converging to the stable periodic solution at low frequency.

5.2. Case Q below threshold

When $Q \leq 6.8$ there are actually two possible scenarios for the low frequency branch: (i) two coexisting low frequency branches and (ii) just one branch left since the other has been annihilated after the collision of F1 with F2. We assume that no perturbation is introduced so that the behavior of the cantilever is actually the same for both of the two sub-cases. An example of the resulting bifurcation diagrams are shown in Figs. 7(a) and 7(b), where the potential upper low frequency branch is omitted for simplicity.

In this case the solution always evolves along the LF branch until point F3 where the jump to the HF branch is triggered by the fold in that point. Concerning the jump from high to low, the same considerations given for the previous case hold. This time the hysteresis region expands between points H and F3.

5.3. Continuation of jumps in the $\overline{\tau} - Q$ plane

DDE-Biftool is able to continue some kind of bifurcations of periodic orbits in two parameters by setting an initial guess of the bifurcation point. This feature is helpful since it allows one to predict the jumps by making continuation with respect to both $\overline{\tau}$ and Q, simultaneously. In Fig. 8 we show how the main bifurcation points of Figs. 5 and 7 are shifted when $Q \in (4, 11)$.

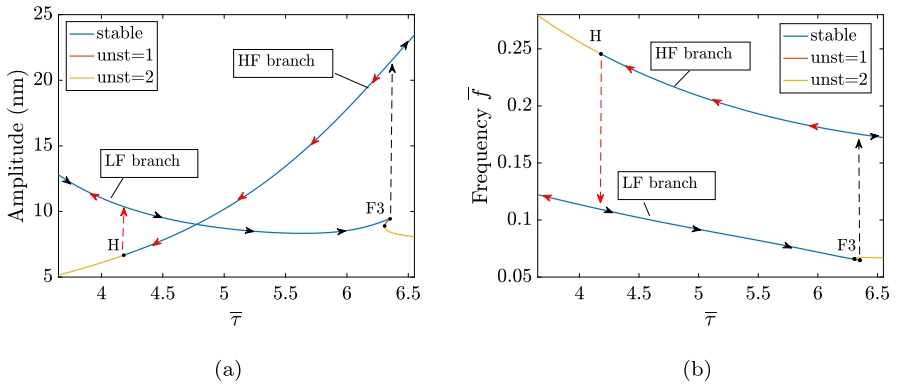

Fig. 7. Bifurcation diagrams in terms of amplitude (a) and normalized frequency $\overline{f}$ (b) when $Q \leq 6.8$.

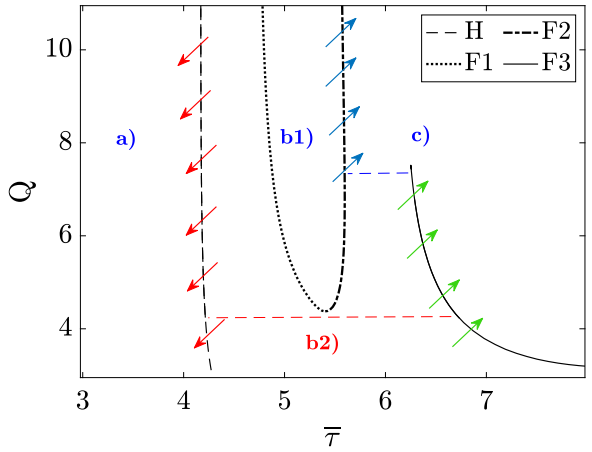

Fig. 8. Bifurcation curves and related jumps in $\overline{\tau} - Q$ plane. The plane has also been divided in sub-regions, each of them characterized by the presence of different solutions.

Starting from the left, we first have the curve representing how the secondary Hopf bifurcation in H moves as Q is varied. Then, we have the two intersecting curves describing the folds in F1 and F2. The rightmost curve is, instead, the evolution of the fold in point F3 which exists only if Q is sufficiently low.

For a better understanding, we briefly bring back the results of Section 4 in Fig. 8. From that analysis, we can easily divide the $\overline{\tau} - Q$ plane in three main sub-regions: (a), (b) and (c). Region (a) is characterized by the concurrent presence of an unstable quasi-periodic HF branch and a stable periodic LF branch. In region (b) there is always a stable periodic limit cycle at high frequency, but, concerning the low frequency branch, we know there are actually two main possible scenarios. Given this fact, region (b) has been divided in other two sub-areas: in (b1) there are up to three stable limit cycles with two of them asymmetric and the other symmetric; region (b2) contains instead just one stable (symmetric) limit cycle. Region (c) is the opposite of region (a). In fact, there is the simultaneous presence of LF and HF branches, but this time just the latter branch is stable.

Having those bifurcation curves on $\overline{\tau} - Q$ plane and those regions, we can finally add to Fig. 8 the arrows embodying the jumps experienced by the cantilever as $\overline{\tau}$ is swept up and down.

The jumps from LF to HF branch, which, according to Q, may be caused by the fold in F2 or F3, are displayed with two different colors in order to allow a better understanding if the LF branch is symmetric or not. In particular, blue arrows represent the jumps from the asymmetric branches, while the green ones define those jumps departing from the symmetric branch. The red arrows, instead, describe the jump in the reverse direction (from HF to LF branch) that only follows the H curve. Notice that the space dividing horizontally the red and blue/green arrows defines the hysteresis region, and that its width is greater as Q decreases.

6. Discussion

The dynamics of system (7) is characterized by sudden jumps which depend both on the delay $\overline{\tau}$ and the quality factor Q, as shown in Fig. 8. Now, the properties of the fluid, such as the viscosity and density of the medium, strongly affect

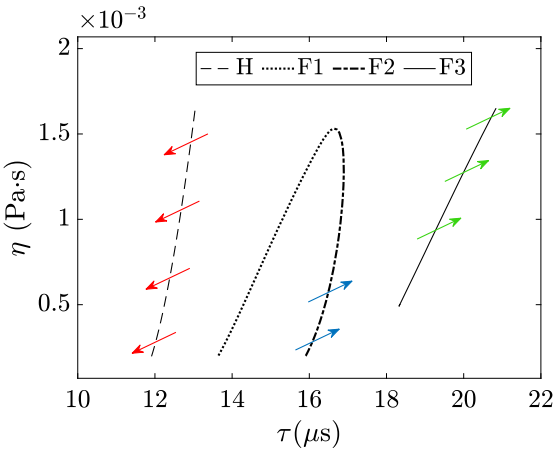

Fig. 9. Bifurcation curves and related jumps in the $\tau - \eta$ plane.

the quality factor Q. Although there are alternatives ways for modeling hydrodynamics forces [22], we used the method proposed in [23,24]. The two parameters m and c of Eq. (1) can be respectively split into two terms each: $m = m_0 + m_A$ and $c = c_0 + c_A$ where m_0 is the mass of the cantilever, c_0 is the intrinsic damping, while m_A and c_A are the added mass and damping due to the interaction of the beam with the viscous fluid. These two latter contributions depend on the viscosity η and density ρ_f of the medium, together with the oscillation frequency which is assumed to be equal to the cantilever natural frequency ω_n, since the exact relation is not relevant for the jumps to occur [6]. Q can be expressed as a function of the mass m and damping c as follows:

$$Q = \frac{m}{c}\omega_n \tag{9}$$

Therefore, any change in η or ρ_f causes a variation in m_A and c_A which, in turn, modify Q. As a consequence, if the relation among the various parameters is known, it is possible to represent the bifurcation diagrams of the previous sections with respect to different parameters. Indeed, similarly to Fig. 8, we can easily plot the bifurcation curves of points H, F1, F2 and F3 on the $\tau - \eta$ plane, as reported in Fig. 9. Notice that in this case the delay has been considered with its original μs units, as done in [6]. Once again the blue and green arrows indicate jumps from LF to HF branch (blue for asymmetric LF branch, green for symmetric LF branch), and the red arrows the jumps from HF to LF branch. As expected, the position of the jumps is sensitive to η, suggesting that a sensor based on the detection of the jumps for the measurement of the rheological properties is possible. Furthermore, also the hysteresis region, (i.e. the separation between red and blue/green arrows for the same η) is visible confirming the results reported in [6]. Nevertheless, the physical realization of such a sensor introduces some unavoidable differences than system (7) implemented in DDE-Biftool as, for example, the use of a phase shifter (PS) to control the delay of the loop. In [6] the authors studied the response for four different viscous fluids with a quality factor $Q \in [4, 5]$. According to our findings, for that range of Q, the jump from low to high frequency is due to the fold bifurcation in point F3 of Fig. 2e, while the jump in the reverse direction is triggered by the secondary sub-critical Hopf bifurcation in point H, see Fig. 4(a). For the sake of clarity, we report in Fig. 10 the comparison between the frequencies acquired experimentally in [6] and the theoretical predictions obtained by using DDE-Biftool and a Simulink model for a cantilever oscillating in water. In Simulink we implemented explicitly the dynamics of the PS according to Eq. (2) rather than considering a pure delay so that a more realistic model could have been taken into account. As said previously, the effect of the variable delay can be reproduced by changing the time constant γ of the PS. Of course, the responses computed using Simulink (and the experimental data as well) are not directly comparable with the theoretical results derived with DDE-Biftool since they are not expressed in function of τ but in terms of γ. Hence, for any given γ, the following equation was used to compute the equivalent delay τ_{PS} added into the loop by PS

$$\omega_n \tau_{PS} = 2\,\mathrm{arctg}(\omega_n \gamma) \tag{10}$$

which ensures that the phase shifter is providing the same phase delay around the cantilever oscillation frequencies. In DDE-Biftool we preferred to work with a pure delay for three main reasons: (i) to speed up the simulations, (ii) have a more generic system and (iii) less derivatives to define.

The two theoretical models agree quite well. In particular, the frequencies and jumps computed by Simulink are pretty close to the predictions of DDE-Biftool, although a perfect superposition cannot be expected since the two models are not exactly equivalent. Concerning the experimental data, the frequencies are quite close to the theoretical values, but both the jumps are anticipated with respect to the estimated ones. This is due to some experimental aspects that cannot be properly considered in this simplified theoretical model:

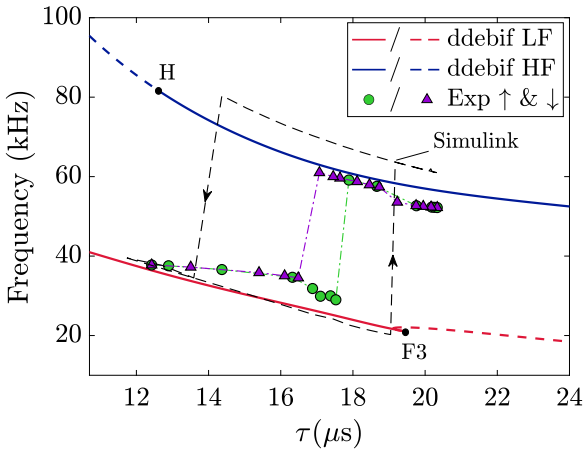

Fig. 10. Comparison between DDE-Biftool (continuous lines), Simulink model (black dashed lines) and the experimental data (markers) acquired sweeping up and down the amount of phase shift, which causes a variation in the total delay τ.

- Q is kept fixed whereas experimentally it changes its value after the jumps. In fact, recall that Q depends on m_A and c_A which vary with the oscillation frequency;
- The presence of noise in the real circuit which we neglected both in Simulink and DDE-Biftool. The noise always causes an anticipation of the jumps since it may lead to a perturbed solution which is grabbed inside the basin of a different attractor;
- The experimental data are influenced on the velocity with which the phase is varied. If this variation happens too fast the cantilever looses its stability earlier, jumping towards the nearest stable attractor.

7. Conclusions

In this paper we studied the stability of periodic orbits for a self-excited microcantilever oscillating in a viscous fluid with a variable delay by using DDE-Biftool, a Matlab package able of performing numerical bifurcation analysis of DDEs. We first normalized the system so that the study could have been carried out on a more general and simpler model. Then, we performed our analysis with DDE-Biftool. Here the main results: the jump from high to low frequencies (once the delay is swept down), is due to a secondary sub-critical Hopf Bifurcation; the jump in the reverse direction for sweeping up the delay is highly influenced by the environment. This jump is always caused by the presence of a fold bifurcation, but the departing low frequency branch can be either symmetrical (if Q is too low) and asymmetrical (when Q is high). The pitchfork bifurcation producing the asymmetric branches can be both supercritical or sub-critical, it depends on Q. The current analysis explains the causes of the phenomena seen experimentally (jumps and the associated hysteresis region), but it also confirms how it may be possible to create sensors, for the rheometry of the fluids, based on the detection of those phenomena.

CRediT authorship contribution statement

Matilde Gelli: Writing – original draft, Methodology, Software, Writing – review & editing. **Joao Mouro:** Conceptualization, Funding acquisition, Data curation, Validation. **Paolo Paoletti:** Conceptualization, Investigation, Methodology. **Bruno Tiribilli:** Data curation, Funding acquisition, Validation. **Michele Basso:** Conceptualization, Supervision, Writing – review & editing.

Declaration of competing interest

The authors declare that they have no known competing financial interests or personal relationships that could have appeared to influence the work reported in this paper.

Data availability

Data will be made available on request

References

[1] Dufour I, Maali A, Amarouchene Y, Ayela C, Caillard B, Darwiche A, et al. The microcantilever: A versatile tool for measuring the rheological properties of complex fluids. J Sensors 2012;2012(1). http://dx.doi.org/10.1155/2012/719898.

[2] Boskovic S, Chon JWM, Mulvaney P, Sader JE. Rheological measurements using microcantilevers. J Rheol (N. Y. N. Y). 2002;46(4):891. http://dx.doi.org/10.1122/1.1475978.

[3] Mouro J, Tiribilli B, Paoletti P. A versatile mass-sensing platform with tunable nonlinear self-excited microcantilevers. IEEE Trans Nanotechnol 2018;17(4):751–62. http://dx.doi.org/10.1109/TNANO.2018.2829404.

[4] Urasaki S, Yabuno H, Yamamoto Y, Matsumoto S. Sensorless self-excited vibrational viscometer with two Hopf bifurcations based on a piezoelectric device. Sensors 2021;21:1127. http://dx.doi.org/10.3390/s21041127.

[5] Mouro J, Tiribilli B, Paoletti P. Measuring viscosity with nonlinear self-excited microcantilevers. Appl Phys Lett 2017;111:144101. http://dx.doi.org/10.1063/1.4995386.

[6] Mouro J, Paoletti P, Basso M, Tiribilli B. Measuring viscosity using the hysteresis of the non-linear response of a self-excited cantilever. Sensors 2021;21:5592. http://dx.doi.org/10.3390/s21165592.

[7] Yabuno H, Higashino K, Kuroda M, Yamamoto Y. Self-excited vibrational viscometer for high-viscosity sensing. J Appl Phys 2014;116(12). http://dx.doi.org/10.1063/1.4896487.

[8] Basso M, Paoletti P, Tiribilli B, Vassalli M. Modelling and analysis of autonomous micro-cantilever oscillations. Nanotechnology 2008;19(47). http://dx.doi.org/10.1088/0957-4484/19/47/475501.

[9] An L, Yabuno H. Self-excited oscillation produced by a phase shift: Linear and nonlinear instabilities. Nonlinear Dyn 2021. http://dx.doi.org/10.1007/s11071-021-07060-4.

[10] Engelborghs K, Luzyanina T, Roose D. Numerical bifurcation analysis of delay differential equations using DDE-BIFTOOL. ACM Trans Math Software 2002;28(1):1–21.

[11] Engelborghs K, Luzyanina T, Samaey G. DDE-BIFTOOL V. 2.00: A Matlab package for bifurcation analysis of delay differential equations. Technical report, 2001, p. TW–330.

[12] Sieber J, Engelborghs K, Luzyanina T, Samaey G, Roose D. DDE-BIFTOOL v. 3.1.1 Manual — Bifurcation analysis of delay differential equations, http://arxiv.org/abs/1406.7144.

[13] Bosschaert M, Miller B, Sieber J, Kuznetsov YA. DDE-Biftool: Bifurcation analysis for delay-differential equations, version 3.1.1 [Computer software], https://sourceforge.net/projects/ddebiftool/.

[14] Van Leeuwen R, Karabacak DM, Van der Zant HSJ, Venstra WJ. Nonlinear dynamics of a microelectromechanical oscillator with delayed feedback. Phys Rev B 2013;88. http://dx.doi.org/10.1103/PhysRevB.88.214301.

[15] Strogatz SH. Nonlinear dynamics and chaos with applications to physics, biology, chemistry and engineering. CRC Press; 2018.

[16] Nayfeh AH, Balakumar B. Applied nonlinear dynamics. Analytical, computational and experimental methods, Wiley-VCH; 2004.

[17] Ghayesh MH, Farokhi H, Gholipour A, Hussain S. On the nonlinear mechanics of layered microcantilevers. Internat J Engrg Sci 2017;120:1–14. http://dx.doi.org/10.1016/j.ijengsci.2017.06.012.

[18] Tabaddor M. Influence of nonlinear boundary conditions on the single- mode response of a cantilever beam. Int J Solids Struct 2000;37:4915–31. http://dx.doi.org/10.1016/S0020-7683(99)00197-3.

[19] Vidyasagar M. Nonlinear systems analysis. 2nd ed.. Englewood Cliffs, NJ: Prentice-Hall; 1993.

[20] Paoletti P, Basso M. Analysis of oscillating microcantilever dynamics: A floquet perspective. Proc IEEE Conf Decis Control 2013;360–5. http://dx.doi.org/10.1109/CDC.2013.6759908.

[21] Gelli M, Mouro J, Paoletti P, Tiribilli B, M. Basso. Bifurcation analysis and complex phenomena in self-excited microcantilevers, [computer software]. 2023, https://github.com/MatildeGelli/Bifurcation-analysis-and-complex-phenomena-in-self-excited-microcantilevers.git.

[22] Ande R, Gutschmidt S, Sellier M. Non-linear finite-amplitude oscillations of the large beam arrays oscillating in viscous fluids. J Appl Phys 2022;132:174904. http://dx.doi.org/10.1063/5.0106293.

[23] Sader JE. Frequency response of cantilever beams immersed in viscous fluids with applications to the atomic force micro- scope. J Appl Phys 1998;84(1):64–76. http://dx.doi.org/10.1063/1.368002.

[24] Maali A, Hurth C, Boisgard R, Jai C, Cohen-Bouhacina T, Aim JP. Hydrodynamics of oscillating atomic force microscopy cantilevers in viscous fluids. J Appl Phys 2005;97(7):2005. http://dx.doi.org/10.1063/1.1873060.